European Journal of Pharmaceutics and Biopharmaceutics 141 (2019) 180–190

Contents lists available at ScienceDirect

European Journal of Pharmaceutics and Biopharmaceutics

journal homepage: www.elsevier.com/locate/ejpb

Research paper

Peptide-mediated delivery of therapeutic mRNA in ovarian cancer

Dirk van den Brand[a,b], Mark A.J. Gorris[c], Alexander H. van Asbeck[a,1], Emma Palmen[a], Inge Ebisch[d], Harry Dolstra[e], Mattias Hällbrink[f], Leon F.A.G. Massuger[b], Roland Brock[a,*]

[a] Dept. of Biochemistry, Radboud Institute for Molecular Life Sciences (RIMLS), Radboud University Medical Center, Geert Grooteplein 28, 6525 GA Nijmegen, the Netherlands
[b] Dept. of Obstetrics and Gynaecology, Radboud University Medical Center, Geert Grooteplein 10, 6525 GA Nijmegen, the Netherlands
[c] Department of Tumor Immunology, Radboud Institute for Molecular Life Sciences (RIMLS), Radboud University Medical Center, Geert Grooteplein 28, 6525 GA Nijmegen, the Netherlands
[d] Department of Obstetrics and Gynaecology, Canisius Wilhelmina Hospital, Weg door Jonkerbos 100, 6532 SZ Nijmegen, the Netherlands
[e] Laboratory of Hematology, Department of Laboratory Medicine, Radboud University Medical Center, Geert Grooteplein 10, 6525 GA Nijmegen, the Netherlands
[f] Department of Neurochemistry, Stockholm University, Sweden

ARTICLE INFO

Keywords:
Drug delivery
Messenger RNA
Cell-penetrating peptides
Ovarian cancer
Nanomedicine

ABSTRACT

Ovarian cancer is the most lethal gynecological malignancy in the developed world. In spite of intensive research, the mortality has hardly decreased over the past twenty years. This necessitates the exploration of novel therapeutic modalities. Transient protein expression through delivery of mRNA is emerging as a highly promising option. In contrast to gene therapy there is no risk of integration into the genome. Here, we explore the expression of mRNA in models of ovarian cancer of increasing complexity. The cell-penetrating peptide (CPP) PepFect 14 (PF14) was used to formulate CPP-mRNA nanoparticles. Efficient expression of a reporter protein was achieved in two-dimensional tissue cultures and in three-dimensional cancer cell spheroids. PF14 nanoparticles greatly outperformed a lipid-based transfection agent *in vivo*, leading to expression in various cell types of tumor associated tissue. Protein expression was restricted to the peritoneal cavity. Messenger RNA expression across different cell types was confirmed in primary ovarian cancer explants. As ovarian cancer is confined to the peritoneal cavity in most cases, the results create the basis for applications in which the tumor microenvironment is transiently modified through protein expression.

1. Introduction

Epithelial ovarian cancer (EOC) is the most lethal gynecological malignancy in the developed world, and the sixth leading cause of cancer mortality in women [1]. Since the tumor readily distributes throughout the abdominal cavity without causing any symptoms, it is often only discovered when widespread metastases are present. In an advanced stage, EOC therapy consists of cytoreductive surgery and adjuvant chemotherapy in order to remove as much of the tumor as possible. However, (micro)metastases persevere and tumor recurrence is almost inevitable. Median progression-free survival (PFS) of EOC is only 18 months, and resistance to chemotherapy is common after tumor recurrence [2].

Emerging novel therapies are the tyrosine kinase inhibitor cediranib and the monoclonal antibody bevacizumab that both inhibit angiogenesis. Cediranib significantly increased PFS in combination with chemotherapy [3]. Combination therapy of bevacizumab with chemotherapy also showed increased PFS in newly diagnosed and platinum resistant ovarian cancer [4,5]. It furthermore showed an increase in overall survival in a subcategory of poor-prognosis patients [5]. Poly (ADP-ribose) polymerase (PARP) inhibitors are another class of drugs that are currently under investigation and olaparib showed increased PFS in platinum-sensitive cases [6]. Despite the increase in PFS, however, none of these therapies yield increased overall survival. As a consequence, novel therapeutic options are urgently needed.

Remarkably, extraperitoneal metastases of ovarian cancer are only observed in 12–33% of the patients diagnosed with EOC [7]. This trait is exploited with the use of intraperitoneal (IP) chemotherapy, in which

* Corresponding author at: Dept. of Biochemistry (286), Radboud Institute for Molecular Life Sciences, Radboud University Medical Center, Geert Grooteplein 28, 6525 GA Nijmegen, the Netherlands.
E-mail addresses: Dirk.vandenBrand@radboudumc.nl (D. van den Brand), Mark.Gorris@radboudumc.nl (M.A.J. Gorris), Sander.vanAsbeck@radboudumc.nl (A.H. van Asbeck), Emma.Palmen@radboumc.nl (E. Palmen), I.Ebisch@cwz.nl (I. Ebisch), Harry.Dolstra@radboudumc.nl (H. Dolstra), Leon.Massuger@radboudumc.nl (L.F.A.G. Massuger), Roland.Brock@radboudumc.nl (R. Brock).
[1] Current address: Mercurna BV, RE0333, Kloosterstraat 9, 5349 AB Oss, the Netherlands.

https://doi.org/10.1016/j.ejpb.2019.05.014
Received 31 January 2019; Received in revised form 13 May 2019; Accepted 15 May 2019
Available online 16 May 2019
0939-6411/

a catheter through which chemotherapy can be applied is left after complete or optimal debulking surgery. This therapy has shown benefit for PFS. In pre-clinical research, IP delivery of nanomedicines has also been explored. This includes IP delivery of small interfering RNA (siRNA) [8–15].

Next to downregulation of protein expression by RNA interference, protein induction by gene delivery has been studied for more than 25 years [16]. While this approach is mostly directed towards reconstitution of expression of defective genes, it has also been used for expression of proteins in cancer therapy. Examples regarding ovarian cancer include the induction of herpes simplex virus thymidine kinase (HSV-TK) and the restoration of P53 and BRCA-1 function [17–19].

One of the obstacles in DNA-based gene therapy is random insertion into the host genome which can induce carcinogenesis [20]. Furthermore, expression can last for uncontrolled periods of time, which is not desired in an acute intervention. Messenger RNA (mRNA) is emerging as a promising alternative that yields a transient protein expression [21]. The focus of this field is still in the area of vaccination, even though the feasibility of therapeutic protein expression, also in large animals, has been demonstrated and clinical trials are underway [22–25].

As for any oligonucleotide-based therapy, the application of mRNA critically depends on efficient delivery vectors. These vectors have to protect the mRNA from enzymatic degradation and mediate efficient cellular uptake and endosomal release. In addition, they also need to shield the mRNA from recognition by the innate immune system [21,26]. Various polymer and lipid-based delivery systems have been explored [26,27]. In most cases, the oligonucleotides are packaged into nanoparticles through non-covalent, charge-driven interactions with a cationic or ionizable delivery agent. Following cellular uptake, induction of efficient endosomal escape is a distinctive characteristic of active delivery vectors [28].

For mRNA-based therapeutic protein expression the focus has been on lipid nanoparticles (LNPs) [29]. By comparison, the (pre-)clinical development of polymers for mRNA delivery is lagging behind. This may be attributed to the fact that an increase in uptake efficiency often correlates with an increase in toxicity as for example for polyethyleneimine [30]. Furthermore, either efficient breakdown and/or excretion have to be ensured. Cell-penetrating peptides (CPPs) constitute an interesting option that combines a low molecular weight with efficient proteolytic break-down. CPPs are a class of mostly cationic peptides of 8–30 amino acids in length that are able to induce cellular uptake of themselves and conjugated cargo [31]. They form nanoparticles with oligonucleotides through non-covalent interactions. Cellular uptake has little predictive power for cytosolic delivery of oligonucleotides, and only few CPPs yield efficient cytosolic oligonucleotide delivery [32]. One CPP with superior delivery capacity for antisense oligonucleotides, siRNA, and plasmid DNA (pDNA) *in vitro* and *in vivo* is PepFect 14 (PF14) [33–36]. This cationic amphipathic CPP consists of 21 amino acids, of which 5 are positively charged, and comprises an N-terminal stearylation.

Regardless of the incorporation of targeting moieties, oligonucleotide polyplexes and LNPs show a strong propensity for liver targeting [12,14,37–40]. Combining CPPs with targeting modalities such as peptides shows only limited success in changing the biodistribution [41]. Therefore, we propose an intraperitoneal approach, akin to intraperitoneal chemotherapy, for exploring the feasibility of mRNA delivery in ovarian cancer. As a basis for future therapy design, we wanted to learn which cell types would be reached in the heterogeneous context of a tumor *in vivo*. Based on the superior characteristics of PF14 for oligonucleotide delivery we chose this CPP for formation of mRNA nanoparticles. For comparison, we selected a commercial lipid-based transfection agent. Following the demonstration that both agents yielded mRNA-dependent protein expression in two-dimensional tissue cultures and three-dimensional tumor spheroids, we assessed protein expression in an intraperitoneal mouse model of ovarian cancer and in human tumor explants. For the murine model, nanoparticles were injected intraperitoneally.

PF14 nanoparticles targeted the tumor but not exclusively the tumor cells within the tumor. Reporter proteins were observed in fibroblasts, tumor cells, and immune cells. The lipid-based formulations did not show any uptake or translation in the xenograft model. Furthermore, there was no expression outside the abdominal cavity. As a consequence, we consider intraperitoneal mRNA delivery a highly interesting option to transiently modulate the peritoneal tumor microenvironment (TME).

2. Materials and methods

2.1. Nanoparticle formation

Messenger RNA, coding for either GFP or mCherry, was modified with 5-methoxyuridine, capped using CleanCap, and polyadenylated (Trilink Biotechnologies, San Diego, CA, USA). The length of the mRNA was 996 nucleotides and Cy5-eGFP mRNA contained a 3:1 methoxyuridine ratio with Cy5. PepFect14 was obtained from Pepscan (Lelystad, The Netherlands). Peptide purity was > 95%. The final peptide concentration was 5 μM for all *in vitro* experiments and particles were formed at an N/P ratio of 3, which corresponds to a final mRNA concentration of 2.68 μg/ml.

Particles were formed by a “stream method”. Two separate stock solutions of peptide and mRNA were prepared in MilliQ (MQ) water and aspirated in two pipette tips that were connected with tubing to two 3 ml syringes placed in a PHD ultra-syringe-pump (Harvard apparatus, Holliston, MA, USA). The pipette tips were inserted into a custom-made holder in which a 1.5 ml Eppendorf tube was placed to collect the nanoparticle solution. The angle between both tips was 35°, and the angle between the tips and the tube wall was 45°. The pump was set at an output flow rate of 9 ml/min. Nanoparticles were formed at a concentration 10× higher than the final concentration.

The hydrodynamic radius of the nanoparticles was determined by dynamic light scattering (DLS) using a Zetasizer Nano ZS apparatus (Malvern Instruments, Worcestershire, UK). DLS measurements of the freshly prepared nanoparticle formulations were conducted at 25 °C in MQ with ZEN0040 cuvettes.

The lipid mRNA formulations were prepared with Lipofectamine MessengerMAX Transfection Reagent (LipMM, Invitrogen, ThermoFisher Scientific, Landsmeer, Netherlands) according the manufacturer’s protocol. In short, a 3% (v:v) LipMM solution in Opti-MEM (Invitrogen, Waltham, MA, USA) was used. Messenger RNA was added at a concentration of 10 μg/ml and subsequently diluted 10×, which corresponded to a final mRNA concentration of 1 μg/ml on the cells.

2.2. Monolayer cell culture and transfection

SKOV-3 cells were purchased from the American Type Culture Collection (ATCC) and SKOV-3-GFP/Luc cells were stably transfected in an earlier study [42]. All cells were cultured in complete culture medium: Dulbecco’s Modified Eagle Medium (ThermoFisher) supplemented with 10% fetal calf serum (PAN-Biotech, Aidenbach, Germany) and GlutaMAX (ThermoFisher) in a 37 °C, 5% CO_2 humidified incubator. The medium was refreshed three times per week, and subconfluent cells were maintained as proliferating cultures or seeded for experiments.

For microscopy, 10,000 SKOV-3 cells were seeded in a μ-Slide 8 well (IBIDI, Planegg, Germany) two days prior to the experiment. For flow cytometry, 120,000 or 60,000 cells were seeded respectively 1 or 2 days prior to the experiment. Cells in microscopy slides and in 24-well plates were incubated by diluting PF14/mRNA nanoparticles 1:10 in complete culture medium. The cells were washed after two hours and incubated for an additional 22 h. Unless otherwise stated, all transfections included a non-treated sample, naked mRNA, PF14 formulated mRNA

and mRNA in LipMM.

2.3. Spheroid culture and transfection

Tumor cell spheroids were formed by the hanging drop method as described earlier [43]. In short, SKOV-3 cells were detached with trypsin/EDTA and 10,000 cells were seeded in 30 µl drops hanging from the inverted lid of a petri dish (VWR international, Radnor, PA, USA, 140 × 20.6 mm). Cells were incubated in complete culture medium containing 1.2 mg/ml methylcellulose (M6385, Sigma-Aldrich, Zwijndrecht, Netherlands) with 200 U/ml penicillin/streptomycin (Sigma-Aldrich). Spheroid formation was observed between 48 and 72 h.

Six spheroids per condition were selected and each one was incubated with either 3 µl PF14/mRNA nanoparticle solution or 3 µl LipMM control. For flow cytometry, SKOV-3 spheroids were incubated with Cy5-eGFP mRNA. For confocal microscopy, SKOV-3-GFP/Luc spheroids were transfected with mCherry mRNA. Spheroids were washed after 4 h, transferred to a 1.5% (w:v) agarose-coated 96-well transparent flat bottom plate (Corning, New York, USA), and incubated for an additional 20 h.

2.4. Spheroid clearing and confocal microscopy

Prior to microscopy, spheroids were fixed and cleared with an adjusted version of the SeeDB clearing protocol [44]. The spheroids were transferred from the agarose-coated plate and transferred to an Eppendorf tube, washed twice in PBS, and fixed in 4% PFA for 1 h. They were subsequently incubated in 28.75%, 57.5%, and 115% (w:v) fructose solution with 0.5% (v:v) thioglycerol for 1 h per concentration. The spheroids were transferred to a µ-Slide 8 well prior to the 115% incubation step. Confocal microscopy was performed directly after the last incubation step, or samples were stored at 4 °C for imaging within 3 days.

2.5. Tumor explant culture and transfection

Tumor explants were cultured as described before [27]. In short, fresh ovarian cancer metastases were obtained from three patients undergoing a cytoreductive surgery for a stage IIIC high grade serous adenocarcinoma at the Canisius Wilhelmina Hospital, Nijmegen, The Netherlands.

To allow for oxygen and nutrient diffusion into the tissue, tumor specimens were cut into 300 µm slices with a Leica VT1000 S vibratome (Leica Biosystems, Wetzlar, Germany) using a vibration amplitude of 0.6 mm and frequency of 100 Hz. Speed was adjusted for each sample in order to acquire high-quality sections. The explants were cultured in a 12- or 24-well plate containing complete culture medium with 200 U/ml penicillin/streptomycin, 2.5 µg/ml amphotericin B (Sigma-Aldrich) and 50 µg/ml gentamycin (Sigma-Aldrich). Plates were placed on a shaker in a humidified incubator at 37 °C enriched with 5% CO_2 and incubated over night prior to the start of the experiment.

Ethical approval for this study was provided by the Radboudumc Ethical Committee (dossier number 2016–2636), which granted the use of peritoneal tumor deposits that were regarded as 'left-over material' in accordance with the code of proper secondary use of human tissue in The Netherlands, as established by the Dutch Federation of Medical Scientific Societies.

Tumor explants were incubated with 30 µl of either PF14/Cy5-eGFP mRNA nanoparticles for confocal microscopy imaging or PF14/mCherry mRNA nanoparticles for multiplex immunohistochemistry in a total volume of 300 µl complete culture medium. After 4 h the samples were washed and incubated further for 20 h. The explants were fixed in 4% PFA overnight and imaged by confocal microscopy, or processed further for multiplex immunohistochemistry.

2.6. Xenograft model and transfection

The animal experiment was approved by the Dutch Central Authority for Scientific Procedures on Animals (CCD) and performed according to Dutch and European laws. Fourteen female nude BALB/c mice (BALB/cAnNRj-Foxn1nu/nu, Janvier Labs, Le Genest-Saint-Isle, France) with a starting weight of approximately 20 g were IP injected with 1×10^6 SKOV-3-GFP/Luc cells. Three weeks after tumor inoculation, tumor size was assessed by measuring bioluminescence. The mice were injected IP with 200 µl 15 mg/ml D-luciferin (PerkinElmer, Waltham, MA, USA), anesthetized with isoflurane and bioluminescence was measured after 3 min on an IVIS Lumina (PerkinElmer). Tumor size was assessed by measuring the mean bioluminescence originating from the abdomen. The mice were divided into four groups: high, intermediate, low, and no tumor growth. Animals in the first three groups enrolled in the study. Mice for each group were assigned with the aid of a random sequence generator.

In week four after tumor inoculation, the experiment was performed on the high tumor group, in week five on the intermediate tumor group, and in week six on the low tumor group. The nanoparticles were prepared as described above and diluted 10× in PBS prior to IP injection of 800 µl PBS containing various concentrations of nanoparticles, except for one mouse that was injected with 400 µl in order to test the lowest dose of nanoparticles. PF14 nanoparticles were injected at a final peptide concentration of 10 and 20 µM at an N/P ratio of 3 resulting in total amounts of injected mRNA of 2.15, 4.3 and 8.6 µg. LipMM samples were prepared according to the manufacturer's protocol with 2 µg mRNA. Animals were injected with either eGFP-Cy5 or mCherry mRNA.

The following day, the mice were anesthetized with isoflurane and euthanized with CO_2. The organs were removed, weighed, and organs from mice that had received eGFP-Cy5 mRNA were analyzed for Cy5 fluorescence on the IVIS Lumina (PerkinELmer). After fixation in 4% PFA solution, parts of the tumor and organs were analyzed by confocal microscopy. The tumors of mice that had received mCherry mRNA were subsequently further analyzed with multiplex immunohistochemistry.

2.7. Confocal microscopy

Monolayer and spheroid imaging were performed with a TCS SP5 confocal microscope (Leica Microsystems, Mannheim, Germany). The HCX PL FLUOTAR 20 × 0.50 N.A. or 40 × 0.75 N.A. dry lenses, or 63 × 1.20 N.A. water lens were used. eGFP, mCherry, and Cy5 were excited with the 488 nm line of an argon ion laser, or 594 nm or 633 HeNe lasers. Fluorescence was detected with photomultiplier tube detectors between 500 and 550 nm, 595–540 nm, or 650–690 nm. Confocal z-stacks of entire spheroids were acquired with an inter-slice distance of 5 µm.

Murine samples and tumor explants were imaged with an SP8 SMD (Leica Microsystems). The Leica 40 × 0.85 N.A. and 10 × 0.4 N.A. dry lenses were used. eGFP, mCherry and Cy5 were excited with the 488, 585, and 645 nm laser lines of the white light laser and detection was performed with HyD hybrid detectors at 500–515, 605–615, and 660–670 nm. Overview images were acquired with a tile scan combined with a z-stack, with an inter-slice distance of 10 µm and reconstructed with Leica Application Suite X microscopy software.

2.8. Flow cytometry

Multicellular SKOV-3 tumor spheroids and monolayer cells were cultured and transfected as described above. After 24 h total incubation time, the cells were washed and incubated with trypsin/EDTA (PAN-biotech) until a single cell suspension was obtained. Complete culture medium was added, the cells were centrifuged, re-suspended in PBS and cell-associated fluorescence was measured on a FACSCalibur flow cytometer (BD Bioscience, Erembodegem, Belgium). eGFP was detected using the 488 nm laser for excitation and the 530/30 emission filter for

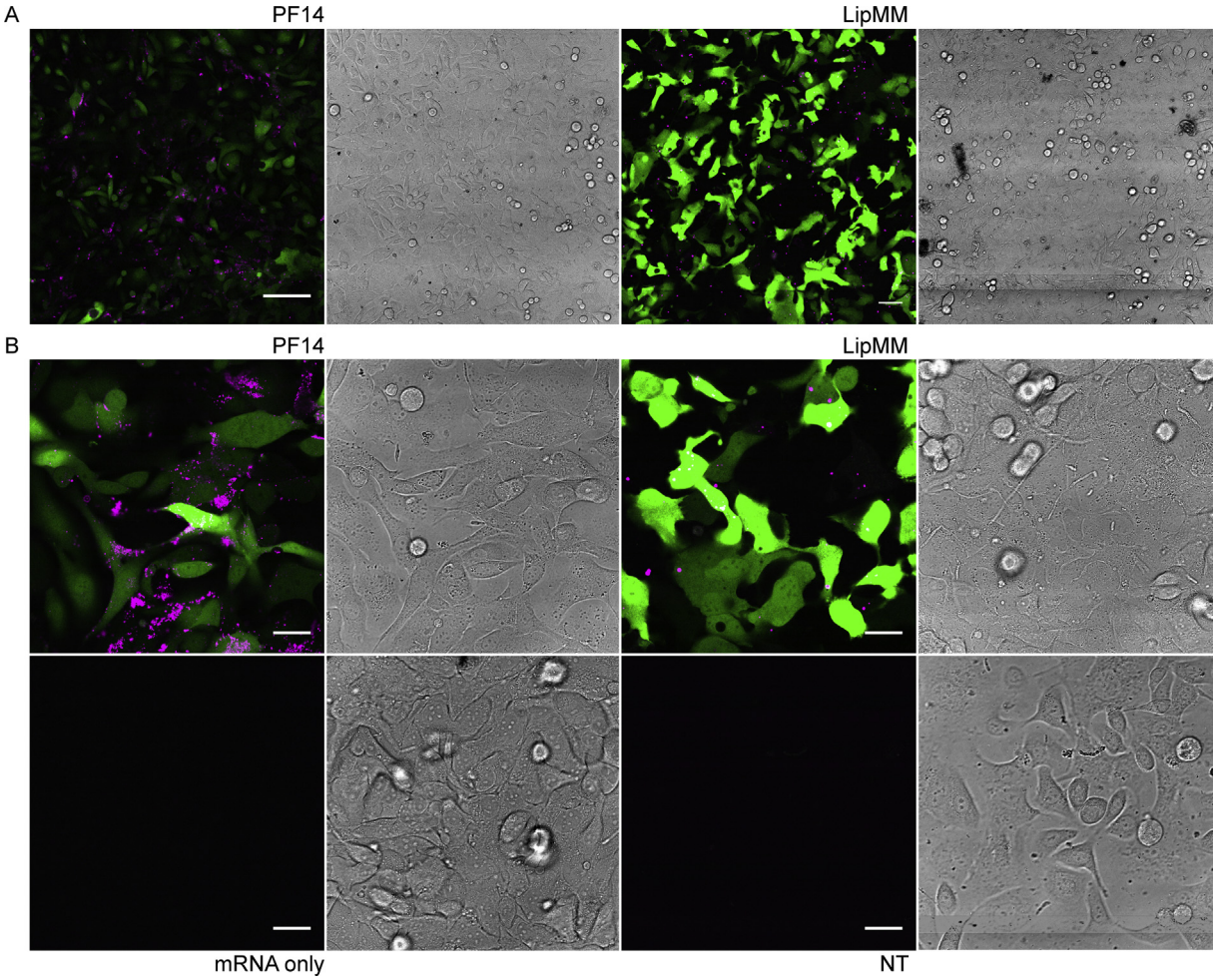

Fig. 1. Uptake and expression of PF14 and LipMM Cy5-eGFP mRNA nanoparticles on a monolayer cell culture of SKOV-3 cells. (A) Overview, scale bar 50 µm. (B) Detailed images of mRNA and eGFP fluorescence, scale bars 25 µm. Cy5 is displayed in magenta, eGFP in green. Brightness and contrast settings were adjusted and a mean filter to reduce noise applied equally in the confocal images. Brightness and contrast settings of the brightfield images were enhanced individually to allow for maximum visibility. (For interpretation of the references to colour in this figure legend, the reader is referred to the web version of this article.)

detection. Cy5 was excited and detected using the 633 nm laser and the 670 nm long pass emission filter.

2.9. Multiplex immunohistochemistry

Tumor samples from different experiments were formalin fixed and paraffin embedded (FFPE). Sections of 5 µm were sliced with a microtome and subjected to five-color multiplex immunohistochemistry (mIHC) in sequential staining cycles using Opal 7-color Automation IHC Kit (NEL801001KT; PerkinElmer) on the BOND RX IHC & ISH Research Platform (Leica Biosystems). A multiplex panel was applied on tissue sections consisting of anti-mCherry 1:1000 (ab167453, polyclonal, Abcam, Cambridge, UK) with Opal 520, anti-αSMA 1:4000 (A2547, clone 1A4; Sigma-Aldrich) with Opal 690, CD45 1:750 (M0701, clone 2B11 + PD7/26; Dako, Santa Clara, CA, USA) with Opal 570 and anti-pan Cytokeratin 1:1500 (ab86734, clone AE1/AE3 + 5D3; Abcam) with Opal 650. Primary antibody incubations were performed for 1 h, secondary antibody Opal Polymer HRP Ms + Rb incubations for 30 min, and Opal reagent incubations for 10 min, all at room temperature. All epitope retrievals and antibody-TSA complex removals were performed using Bond Epitope Retrieval 2 (AR9640, Leica Biosystems). Tissue sections were counterstained with DAPI and mounted in Fluoromount-G (0100-01; SouthernBiotech, Birmingham, AL, USA). Slides were imaged with an Automated Quantitative Pathology Imaging System (Vectra 3.0.5, PerkinElmer). InForm software (Version 2.2.1, PerkinElmer) was used for spectral unmixing and image analysis.

3. Results

3.1. Nanoparticle formation

PF14 nanoparticles were prepared at an N/P ratio of 3 in all experiments. This N/P ratio yielded well-defined, monodisperse nanoparticles with a minimum of excess peptide. Cy5-eGFP and mCherry mRNA which both had the same number of 996 nucleotides formed nanoparticles of the same size. The choice of these two different mRNAs was motivated by the fact that we wanted to use an eGFP-expressing ovarian cancer cell line to relate reporter protein expression to tumor cells for the *in vivo* experiments. For this reason, mCherry mRNA was selected. However, this mRNA was not commercially available in a Cy5-labeled form. The Cy5-labeled eGFP mRNA was therefore used for the correlation of mRNA distribution with protein expression. Successful nanoparticle formation relied heavily on optimal mixing of peptide and mRNA (unpublished data), which was achieved by a stream method that ensured immediate turbulent mixing of both components. Particle size was measured by dynamic light scattering and the use of Cy5 labeled mRNA did not affect particle size. The hydrodynamic diameter of both types of particles was 92 nm independent of the presence of the label. The polydispersity index of both particles was 0.259 and 0.248 (Supplementary Fig. S1). At an N/P ratio of 3 encapsulation of mRNA

into PF14 nanoparticles was 98% as determined by reduction of RiboGreen fluorescence. Incubation with heparin led to a time-dependent recovery of fluorescence (Supplementary Fig. S2). LipMM formulations were prepared according to a protocol provided by the manufacturer. As a consequence, the final amount of mRNA was 2.7 times lower compared to the amount of mRNA used in PF14 experiments. This ratio was consistent throughout all experiments. For all *in vitro* experiments, the nanoparticle concentrations were based on 5 μM peptide.

3.2. mRNA uptake and translation in 2D and 3D tumor models

PF14 has been shown to induce effective cellular uptake of antisense oligonucleotides, siRNA, and pDNA [34–36]. A formulation of PF14 with mRNA, however, has not been studied, before. Therefore, transfection efficiencies of both PF14 and LipMM were first analyzed in a monolayer cell culture of ovarian carcinoma cells using eGFP-Cy5 mRNA.

Cells were incubated with nanoparticles for 2 h, washed, and incubated in complete culture medium for an additional 22 h. Hereafter, expression was analyzed by confocal microscopy. For samples that were incubated with mRNA only, no Cy5 signal was present and none of the cells expressed eGFP (Fig. 1). Incubation with PF14 nanoparticles, on the other hand, resulted in clusters of high Cy5 intensity, indicating a distribution of mRNA in loose patches across the cell surface and expression of eGFP in a large number of cells. By comparison, in the LipMM sample only few Cy5 clusters were observed that were only partially associated with cells. eGFP expression was higher than in the PF14-treated sample.

As a next step, we probed for protein expression in a 3D spheroid model. A major obstacle concerning confocal microscopy of large and dense objects is signal loss due to light scattering. To be able to optically reconstruct a whole spheroid we used an optical clearing protocol that gives a uniform refractive index within the spheroids [44]. For spheroids formed from SKOV-3-GFP/Luc cells, all cells within the spheroid could be visualized after clearing whereas the maximum scan depth of uncleared spheroids was less than 50 μm (Supplementary Fig. S3). For induction of protein expression, the SKOV-3-GFP/Luc spheroids were incubated with mCherry-mRNA nanoparticles. Spheroids were washed after 4 h, and fixed after a total incubation time of 24 h, followed by clearing and microscopy. mCherry fluorescence was only observed in the outer rim of the spheroids indicating that the nanoparticles did not have the capacity to enter spheroids (Fig. 2). Not all cells on the outer rim were mCherry positive, although PF14 seemed to induce more detectable transfection and protein expression than LipMM. However, we could not decide at this point whether this was due to lack of transfection or partial loss of cells during fixation and clearing.

To further quantify these results, cells were dispersed and analyzed by flow cytometry. In this case, spheroids were grown from SKOV-3 cells that did not express the fusion protein so that also the cell-associated Cy5-mRNA signals could be compared. In comparison, also 2D tissue cultures were taken into account. In 2D, in accordance with microscopy, cells incubated with LipMM nanoparticles showed higher average protein expression (Fig. 3A). However, in the PF14 incubated sample 81% of the cells showed detectable protein production in comparison to only 63% of the cells in the LipMM sample (Fig. 3B). Furthermore, in the LipMM sample a population of roughly 14% of the cells showed Cy5 fluorescence without measurable eGFP production, and 29% showed no uptake of mRNA at all, a population that was nearly absent in the PF14 treated samples (Fig. 3A, C). In 2D, there was no difference in the average Cy5 signal for the two delivery vehicles, indicating that the prominent fluorescence observed by microscopy was only externally associated with cells.

For the spheroids, in accordance with microscopy, only a minor fraction of the cells was reached by the nanoparticles (Fig. 3A). However, around 33% of the cells incubated with PF14 showed Cy5 fluorescence, whereas this was 12% of the cells incubated with LipMM

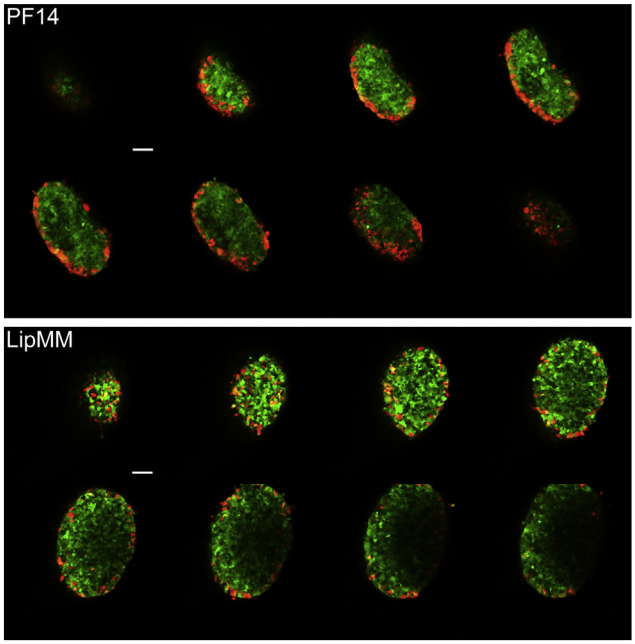

Fig. 2. Cleared SKOV-3-GFP/Luc spheroids that express GFP (green) were transfected with mRNA nanoparticles that induce expression of mCherry (red). Starting from the bottom, a confocal slice was recorded every 25 μm throughout the whole spheroid. Brightness and contrast were equally adjusted and the scale bars denote 100 μm. (For interpretation of the references to colour in this figure legend, the reader is referred to the web version of this article.)

(Fig. 3B). 22% of the cells that were transfected with PF14 and were positive for Cy5 fluorescence also showed detectable eGFP production. In the LipMM transfected sample this was 50%. Still, the total percentage of cells that was double positive for Cy5 and eGFP was slightly higher for PF14 transfected cells (Fig. 3B). Nevertheless, the average eGFP production by Cy5-mRNA positive cells in the LipMM sample greatly exceeded the one of the PF14 sample supporting the hypothesis that the higher intensity observed for PF14 by microscopy was due to partial loss of highly expressing cells at the periphery of the LipMM treated spheroids. Lastly, samples that were incubated with naked mRNA exhibited a slight increase in Cy5-mRNA fluorescence although, as expected, this did not translate in detectable eGFP production.

3.3. mRNA uptake and translation in vivo

The fraction of transfected cells clearly decreased when proceeding from a 2D to a 3D model. However, both models only comprised one cell type and the absence of fluid convection could reduce the capacity of the nanoparticles to penetrate the cell mass. Therefore, we aimed to analyze the biodistribution and expression of the mRNA formulations in a xenograft model carrying an IP tumor of SKOV-3-GFP/Luc cells. Tumor size was assessed three weeks after inoculation by measuring luciferase bioluminescence (Supplementary Fig. S4). Sufficient tumor take was observed in 12 of the 14 animals and the animals were divided into groups of different tumor sizes. Each tumor size group consisted of 4 mice and mice within a group were randomly assigned to the different treatment regimes.

Since we wanted to assess nanoparticle uptake and protein expression by the tumor and different organs, PF14 nanoparticles were prepared with Cy5-labeled mRNA (uptake) and unlabeled mRNA (expression). Due to the limited number of available animals, LipMM was only formulated with mCherry mRNA for the detection of protein expression. The final peptide concentration was 10 μM and a total amount of 8 nmol PF14 with 4.3 μg mRNA was injected IP. As an additional control, an equal amount of Cy5-labeled mRNA was injected without any

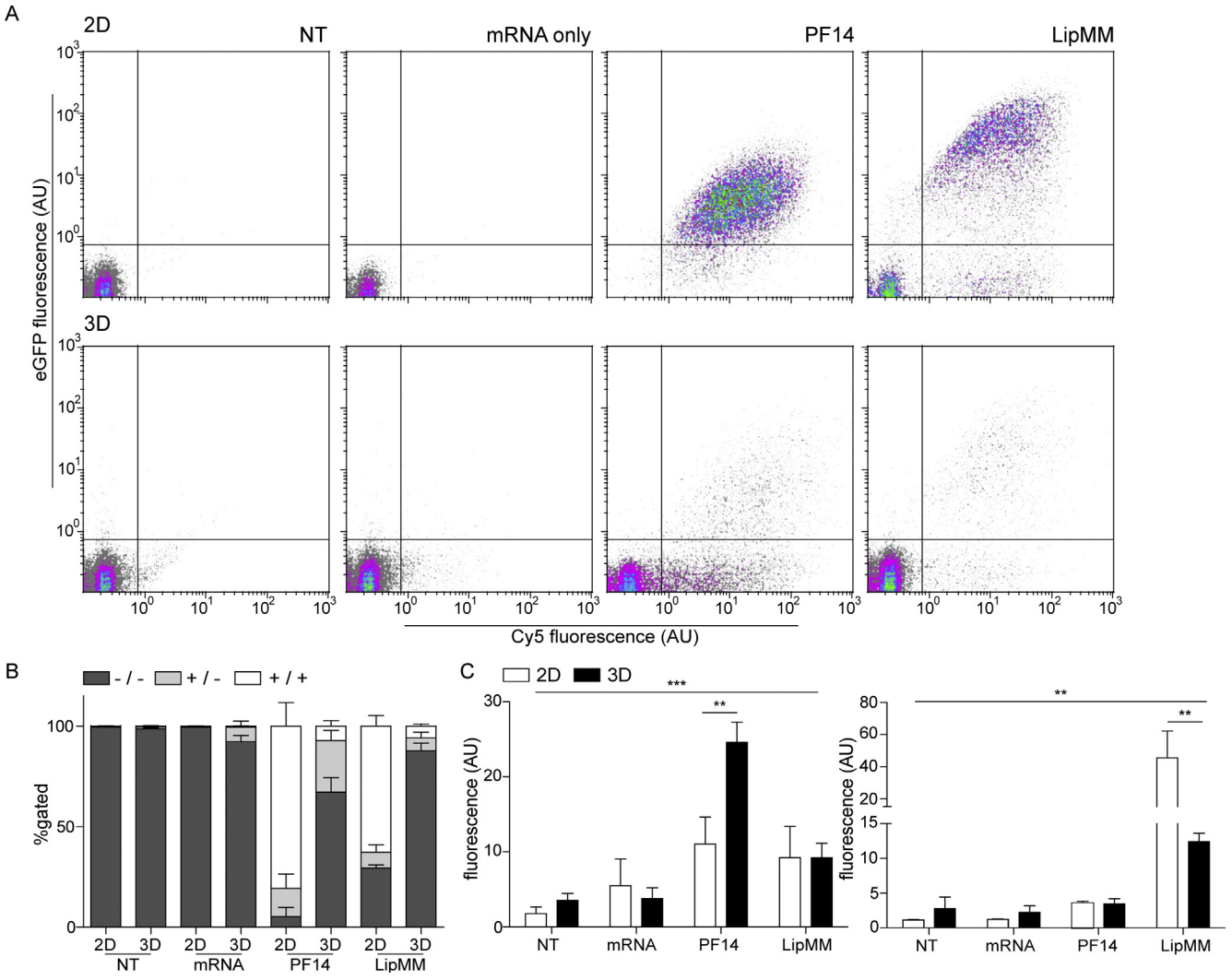

Fig. 3. Flow cytometry of uptake and expression of Cy5-eGFP mRNA nanoparticles. Cell monolayers were incubated for 2 h and spheroids for 4 h. Samples were subsequently washed and after a total incubation time of 24 h trypsinized and single cells were analyzed with flow cytometry to detect cell-associated mRNA fluorescence (Cy5) or mRNA translation of the reporter protein (eGFP). (A) Representative scatter plots after monolayer and spheroid transfection. Depicted plots are from the same experiment. (B) Analysis of the percentage of cells that were either double negative for Cy5 and eGFP fluorescence (−/−), Cy5 positive and eGFP negative (+/−), or double positive for Cy5 and eGFP (+/+). (C) Histograms that depict the fluorescence of the double positive gate. To prevent the analysis of false positive results, fluorescence intensity was only calculated if > 1% of the cells was positive in a certain gate. Left panel depicts Cy5 fluorescence and the increase in the PF14 sample was highly significant compared to the other conditions (***). The right panel shows GFP fluorescence with the LipMM sample having a significantly higher fluorescence compared to PF14 (**). Mean and SEM are shown; N = 4 for 3D PF14 and LipMM; N = 3 for 3D NT and mRNA only; N = 2 for 2D. **, P < 0.01; ***, P < 0.001; 2D, monolayer culture; 3D spheroid culture; NT, non-treated; PF14, PepFect14; LipMM, Lipofectamine MessengerMax.

delivery vehicle. No clinical toxic effects were seen after nanoparticle injection at different concentrations. This was also what we expected since a previous study of PF14 application *in vivo* used much higher concentrations for intravenous injections without any reported adverse events [45]. Twenty four hours after injections, the animals were sacrificed and both, tumor and organs were removed for analysis. Most tumor bulk was observed in the upper left quadrant of the abdomen, and to a smaller extent in the upper right quadrant. Further major tumor depositions were observed on the diaphragm, under the liver, and on the mesentery. Some mice also showed minor tumor deposits at the tumor injection site.

The isolated organs and tumors were analyzed for Cy5 fluorescence. Surprisingly, uptake of nanoparticles was restricted to the tumor as no signal could be detected in any organ (Fig. 4A,B). The tumors of PF14-Cy5 mRNA-treated animals showed significantly higher uptake compared to controls in which Cy5 mRNA only and PF14 with unlabeled mRNA were used (Fig. 4B). The tumors in the control mice were completely negative for Cy5 fluorescence. The brains and intestine showed significant autofluorescence in both the treatment and control groups and the signal was not different between both groups for these organs.

After initial macroscopic assessment, the tumor and organs were fixed and analyzed for Cy5 localization by confocal microscopy. As the tumor cells stably expressed GFP, tumors were easily identified. As apparent from the presence of dark patches, the tumor deposits also contained GFP-negative cells that most likely originated from the host animal. Messenger RNA associated fluorescence was only detected in the tumors of all three PF14-Cy5-mRNA-treated mice, but not in the tumors of control animals or in the other organs (Fig. 4C). Furthermore, the pattern of deposition was similar to the one observed in the spheroid experiments with broadly spread clusters of Cy5 fluorescence. It was furthermore notable that mRNA was solely present on the tumor although not on the tumor cells *per se*. Cy5 fluorescence was also associated with the GFP-negative cells within the tumor.

Protein expression was assessed for mice injected with different concentrations of PF14/mCherry-mRNA nanoparticles and LipMM/

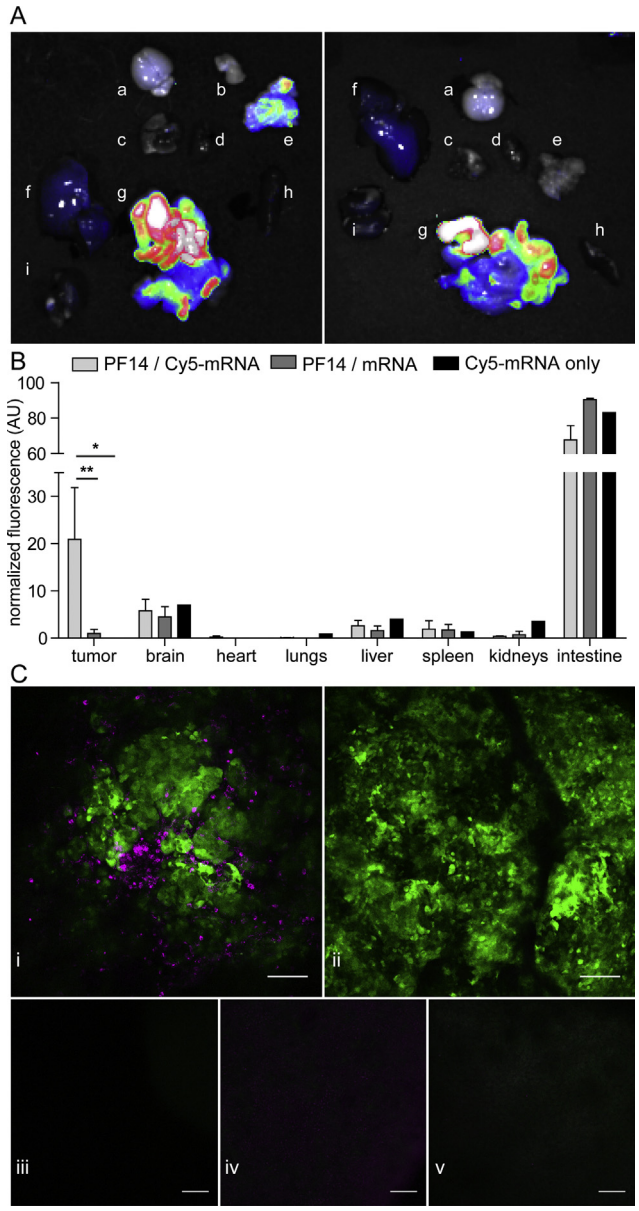

Fig. 4. Assessment of mRNA associated fluorescence after IP injection of PF14 nanoparticles in tumor bearing mice. (A) Cy5 measurement of whole organs and tumor for a mouse treated with PF14/Cy5-labeled mRNA nanoparticles (left) and a mouse treated with PF14/nonlabeled mRNA (right). Fluorescent counts (AU) are shown. a, brain; b, tumor injection site; c, lungs; d, heart; e, tumor; f, liver; g, intestine; h, spleen; i, kidneys. (B) Analysis of fluorescence. A region of interest was drawn around the organ and the mean fluorescence was measured. The signal was normalized to the total fluorescence, since the absolute fluorescent signal varied between different measuring days; N = 2 mice, N = 1 mouse for Cy5-mRNA only. (C) Representative confocal images of the tumor and organs. GFP expressed by tumor cells is shown in green, mRNA in magenta. i, tumor of a mouse treated with PF14/Cy5-labeled mRNA nanoparticles; ii, tumor of a mouse incubated with naked Cy5-labeled mRNA; iii, iv, v, are respectively intestine, spleen, and liver, which were all incubated with PF14/Cy5-labeled mRNA. Background correction, mean filter, and brightness and contrast settings were applied equally for all images. Scale bar denotes 100 μm. (For interpretation of the references to colour in this figure legend, the reader is referred to the web version of this article.)

mCherry-mRNA nanoparticles. After an incubation time of 24 h, the mice were sacrificed and the tumors and organs were fixed in 4% PFA. To our surprise, none of the LipMM treated tumors showed any mCherry expression (Supplementary Fig. S5). On the other hand, the tumors of the mice that had received 4.3 and 8.6 μg PF14-formulated mRNA showed mCherry expression in the tumor (Fig. 5A). No expression was detected in the animal that was treated with 2.7 μg mRNA and the animals that had received naked mRNA (Fig. 5Aiii,Aiv). No mCherry fluorescence could be detected in the intestine, spleen, and liver in any of the animals (Fig. 5B). Outside of the main tumor, the only cells that showed mCherry fluorescence originated from small tumor deposits in the mesentery of the small intestine (Fig. 5B). Clearly, mCherry expression was also observed in GFP negative cells, indicating that other cell types within the tumor were also reached by the PF14-mRNA nanoparticles.

To identify the cell types associated with mCherry expression, multiplex immunohistochemistry was performed for sections of PF14 transfected tumor samples with a positive mCherry signal in confocal microscopy. This included two tumors treated with 4.3 μg mRNA and one with 8.6 μg mRNA. The stained slices were subsequently scanned with multispectral imaging, allowing for optimal differentiation of the different fluorophores. In order to gain information on the most common and important cell types within the tumor that expressed mCherry mRNA, we decided to stain for the tumor cells (pan-cytokeratin), fibroblasts (αSMA), immune cells (CD45), and mCherry. Although nude mice lack a thymus, which makes them immunodeficient due to the absence of mature T lymphocytes, they still possess immune cells from other lineages such as macrophages.

After staining and whole slide microscopy, several areas of interest were selected. The different cell types could be clearly distinguished and a pronounced mCherry signal was visible in the PF14 transfected samples (Fig. 5C). The tumor that was treated with 8.6 μg mRNA showed the highest number of mCherry positive cells. mCherry was found in all the analyzed cell types (Fig. 5C), and based on a semi quantitative analysis we concluded that tumor cells were the most abundant cell type expressing mCherry. In accordance with the spheroid transfection experiments, mCherry positive cells were only found on the outer cell layers of the samples. This shows that the PF14 nanoparticles were unable to penetrate deep into the tumor tissue. Apparently, convection of nanoparticles due to intraperitoneal fluid flow does not increase penetration depth.

3.4. mRNA transfection in tumor explants

The *in vivo* experiments had shown that the PF14 based nanoparticles were able to withstand the conditions present in the abdominal cavity and had the capacity to transfect cells associated with the tumor. Using primary human tumor explants, we further explored the transfection of primary cells. In this model, the 3D architecture and cell types of a clinical tumor are preserved in an *ex vivo* culture system.

Tumor tissue was collected from patients diagnosed with FIGO stage IIIC epithelial ovarian cancer that underwent cytoreductive surgery for EOC. These metastases were subsequently cut into 300 μm thick slices to allow for oxygen and nutrient diffusion. Tumor slices of this thickness are able to remain viable for up to 7 days [46]. Cell proliferation decreased over time from 24% at day two to 9% at day 7 (Supplementary Fig. S6A, Supplementary methods). A live/dead cell stain furthermore revealed that both living and dead cells were present simultaneously in one area of the tumor explant (Supplementary Fig. S6B, Supplementary methods). Tumor explants from three patients were transfected with PF14 and LipMM formulated Cy5-eGFP mRNA at the standard concentration of 5 μM peptide. This included two omental metastases from an interval debulking after neo-adjuvant chemotherapy and one para-aortic lymph node from primary cytoreductive surgery. Samples were washed after 4 h incubation and analyzed after a total incubation time of 24 h. For PF14 nanoparticles, Cy5-eGFP mRNA was present in large patches or smears on the tumor slices (Fig. 6A). Although a similar pattern of mRNA distribution was shown in the earlier experiments, it was even more pronounced in the tumor explants. We therefore hypothesize that the nanoparticles accumulate in

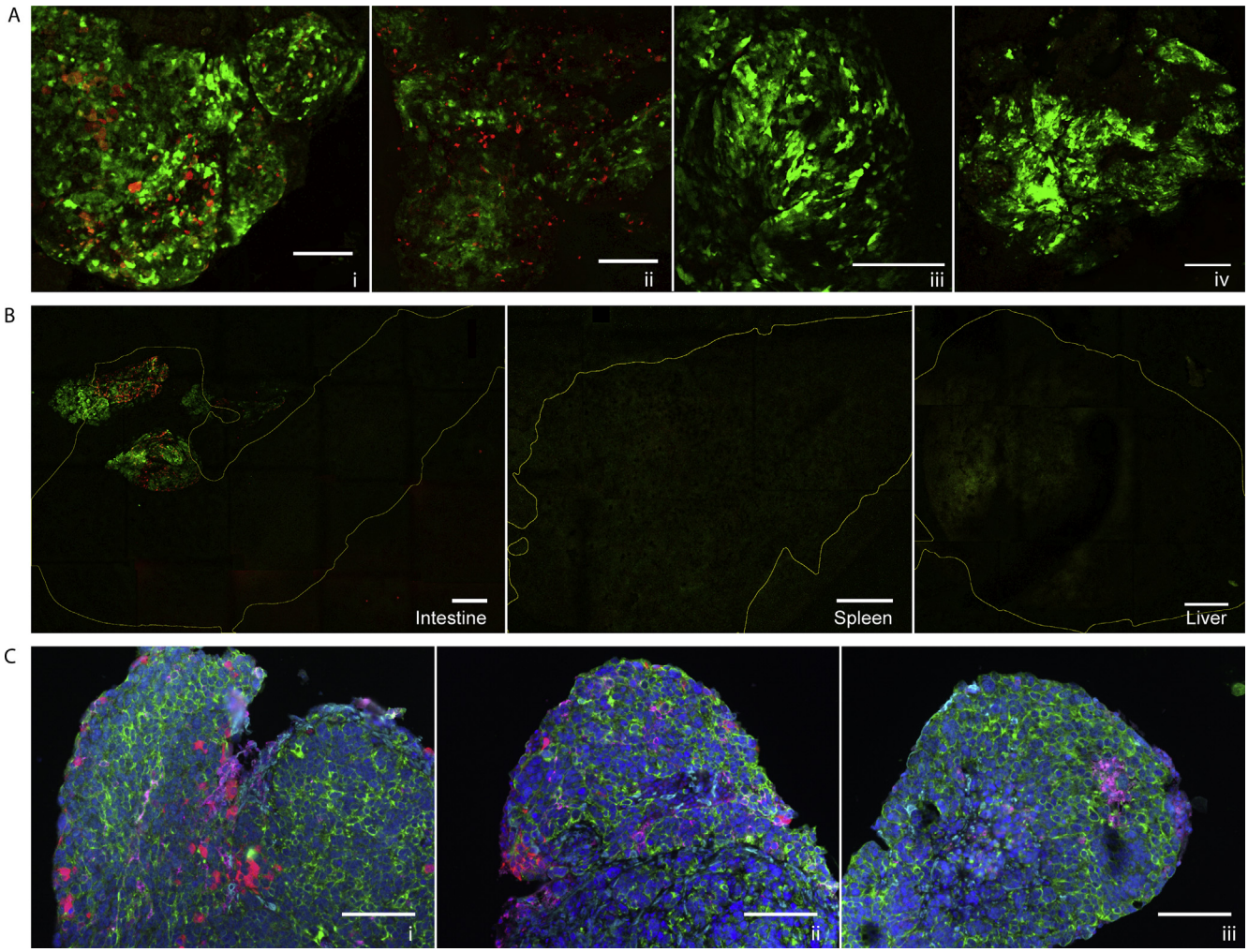

Fig. 5. Microscopy analysis of mouse tumors and organs following intraperitoneal injection of nanoparticles containing mRNA that codes for the fluorescent mCherry protein. (A) Representative confocal microscopy of mouse tumors that were transfected with PF14/mCherry mRNA. The mice were either treated with (i) 20 μM PF14, corresponding to 8.6 μg mRNA, (ii) with 10 μM PF14 corresponding to 4.3 μg mRNA, or (iii) with 10 μM PF14 at half the volume, corresponding to 2.7 μg mRNA; (iv) 4.3 μg mRNA only. The GFP expressing tumor cells are shown in green, and mCherry expression is shown in red. The scale bars denote 250 μm. (B) Representative confocal overview images of the intestine, spleen, and liver from a mouse treated as in A. Macroscopic tumor deposits were visible on the mesentery of the intestine that was imaged. GFP expressing tumor cells are green, and mCherry positive cells are red. The outline of the organs is shown by the yellow line and the scale bars denote 500 μm. (C) Multiplex immunohistochemistry of tumor sections. i, ii, and iii show respectively the same condition as A(i), A(ii), and A(iv); mCherry, red; tumor cells, green; CD45 positive cells, magenta; fibroblasts, cyan; nuclei, blue. The scale bars denote 100 μm. (For interpretation of the references to colour in this figure legend, the reader is referred to the web version of this article.)

the tumor stroma. The distribution of mRNA in the LipMM transfected samples was different. A punctate staining throughout the samples was seen in some samples, whereas other samples did not show any Cy5 fluorescence at all after 24 h. No mRNA associated fluorescence could be retrieved in the controls that were incubated with naked mRNA, indicating that this was degraded and Cy5 released into the incubation medium after 24 h.

Enhanced GFP was visible in most samples that had been incubated with the nanoparticles. Protein production was higher in most LipMM transfected samples than in PF14 transfected samples. However, eGFP expression varied enormously between different patients and even within different samples of the same patient due to heterogeneity in cell density, cell types, and cell viability. For example, two samples from the same patient resulted in different expression levels from the same PF14 or LipMM condition. Furthermore, some tumors mainly consisted of fat cells and these samples did not show any detectable eGFP fluorescence (data not shown).

Due to this heterogeneity, it was difficult to quantify the data. Therefore, a qualitative analysis of cell specificity was performed. For this purpose, explants were incubated with mCherry mRNA in the same way as with Cy5-eGFP mRNA. Following an initial assessment of mCherry expression by confocal microscopy, slices were fixed for multiplex immunochemistry to identify tumor cells, immune cells and fibroblasts. Tumor samples of three patients were processed for multiplex immunohistochemistry. Intentionally, one metastatic lymph node was analyzed next to two tumor depositions. In this way, we wanted to capture transfection in leukocytes or within lymphogenic metastases (Fig. 6B). As expected, the lymph node consisted mainly of immune cells. Of the other two samples, one contained a large fraction of fibroblasts, whereas the other one consisted mainly of tumor cells. All different cell types expressed mCherry and there was no clear preference for any cell type. Preference varied mostly between the patient samples. In one case, for example, only fibroblasts expressed mCherry (Fig. 6Bi). In the other samples, also other cells expressed mCherry. PF14 and LipMM roughly showed the same cellular preference for each patient sample although LipMM showed expression in a larger fraction of the cells in 2 of the 3 patient samples. As before, the penetration of nanoparticles was limited to the outer cell layers and deep penetration

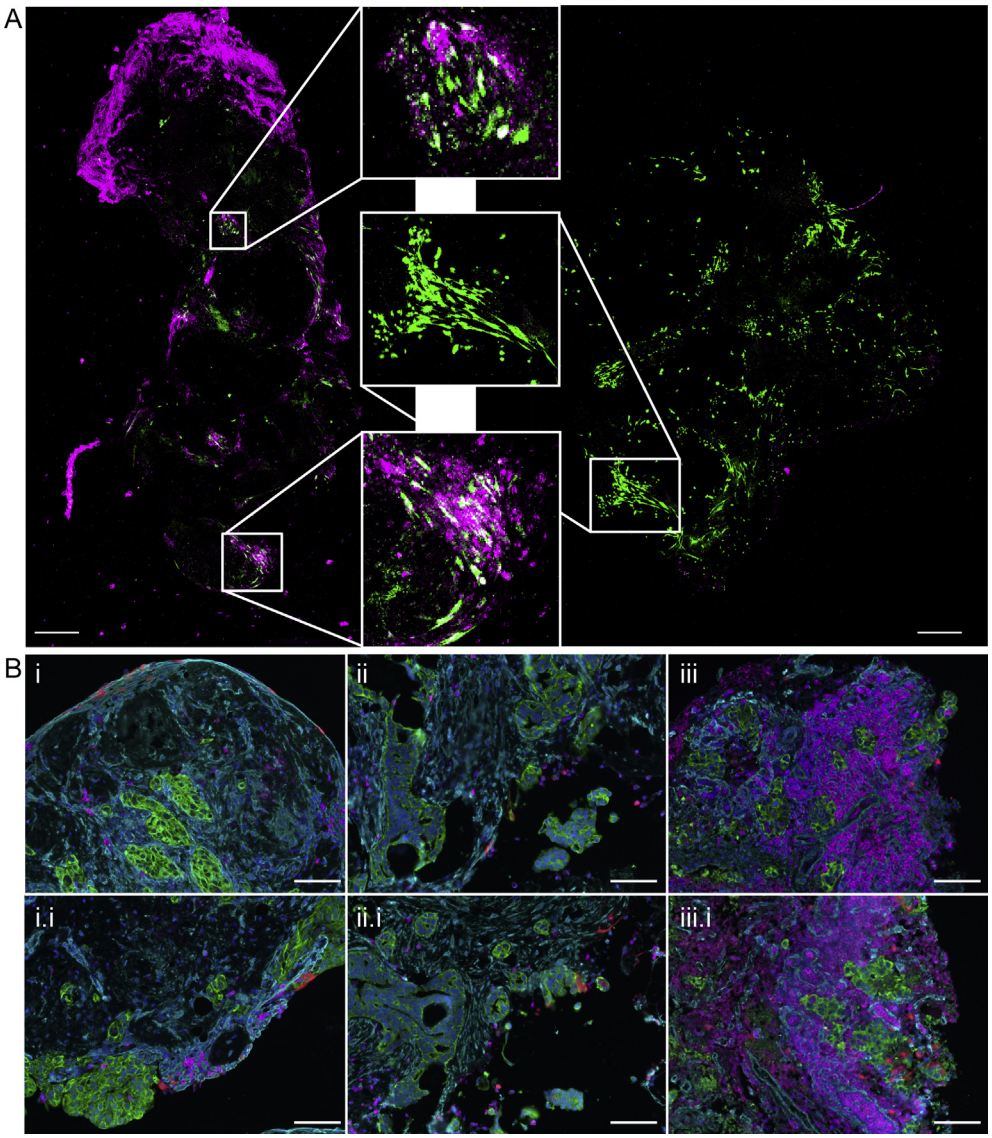

Fig. 6. Representative images of transfection of tumor explants with mRNA formulations. (A) Stitched tile scan and maximum projection of a z-stack of confocal images from the intact tumor explants. Left is PF14 transfected, right is LipMM transfected. Magenta, Cy5-mRNA; Green, eGFP. Scale bars are 500 µm. (B) Immunohistochemistry of mCherry transfected samples. Top images are PF14 transfections and bottom images are LipMM transfections. (i, ii) Omental metastases from two different patients after interval debulking; (iii) lymph node after primary debulking; mCherry, red; tumor cells, green; CD45 positive cells, magenta; fibroblasts, cyan; nuclei, blue. Scale bars denote 100 µm. (For interpretation of the references to colour in this figure legend, the reader is referred to the web version of this article.)

was not observed.

4. Discussion

Here, we demonstrate the feasibility of mRNA delivery in ovarian cancer for a CPP-based delivery vector. For this purpose, we used systems of increasing complexity going from 2D tissue cultures of cancer cells to an *in vivo* model of intraperitoneal ovarian cancer and human tumor explants. In all systems, we compared PF14-based delivery with a standard lipid based transfection agent. Both PF14 nanoparticles and the lipid based transfection agent were able to transfect different cell types *in vitro*. However, only PF14 was able to induce detectable reporter protein expression in a xenograft model of ovarian cancer. Why LipMM also transfected cells in the equally heterogeneous context of human tumor explants cannot be resolved at this point.

The Cy5-labeled PF14 particles were clearly visible with the microscope. However, the flow cytometry data showed that there was hardly any difference in mean uptake between the PF14 particles and LipMM particles. We attribute this observation to two factors. First, the bright fluorescence that was visible in the confocal images of the different experiments was mostly extracellularly and thus washed off when cells were analyzed by flow cytometry. Second, the microscope is less sensitive and the settings were adjusted to the bright extracellular Cy5 clusters. The use of human tumor explants provided highly valuable information on the targeting of different cell types in their original heterogeneous context. However, heterogeneity also posed a challenge as in some cases hardly any tumor cells were present. Also, explants after chemotherapy contained a high number of dead cells. A further streamlining of protocols, for example by preselection of tissues based on histological criteria, would benefit these analyses.

To date, LNPs are the most widely used delivery systems for mRNA even though also various polymers have been explored [26]. In spite of wide-spread application for delivery of other types of oligonucleotides, cell-penetrating peptides, which may be considered short-chain polyamides with excellent degradation capability, have received little attention so far. Udhayakumar et al. (2017) employed an arginine rich CPP with the amphipathic RALA motif for mRNA vaccination [47]. Transfection efficiency of this peptide critically depended on the amphipathic properties of the CPP. Crowley et al. (2015) utilized a polyacridine-polylysine-PEG formulation for delivery of mRNA to the liver in a murine model [48]. PF14 is a CPP with high transfection efficiency for various oligonucleotides. Here, we studied PF14 for the first time as a delivery agent for mRNA.

Upon intravenous injection of PF14/pDNA polyplexes, only PEG-shielded polyplexes achieved reporter protein expression in a subcutaneous glioblastoma xenograft [45]. In contrast, unmodified PF14

particles mainly targeted the lungs of the animals. In the previous study, PEGylation furthermore prevented cationic toxicity [45]. In our study, following intraperitoneal injection, expression was exclusively restricted to the peritoneal cavity and acute toxicity was not observed. Based on the characteristics of the formulation we estimate that Veimann et al. injected 1.5–6 times as much peptide in a concentration that was 10–50 times higher than we did. PF14 could be a promising candidate for clinical development since it achieves efficient mRNA expression with relatively low amounts of mRNA, low peptide concentrations, and low N/P ratios as a high N/P ratio promotes toxicity [49]. At 4.3 μg per mouse, the amount of mRNA was lower than in an earlier study where 7.5 μg luciferase mRNA was complexed with an oligo(carbonate-*b*-*α*-amino ester) carrier for IV or intramuscular (IM) administration [50]. In that study, bioluminescence from the IV injected reporter mRNA was mainly observed in the liver and spleen whereas expression from IM injected mRNA remained restricted to the flank muscle. PF14 nanoparticles specifically targeted the tumor, indicating that on-site delivery of nanoparticles aided passive targeting.

Due to their size, both PF14 and lipid formulations were unable to reach the core of the tumor. As a consequence, only a small fraction of the tumor cells was transfected. Limited tumor penetration is often observed for nanoparticles that are around 100 nm in diameter [51], and efficient penetration is only seen in formulations that are less than 10 nm in size [52]. Thus, decreasing particle size or the addition of tumor penetrating peptides such as iRGD could enhance tumor penetration [53]. Nevertheless, within the TME, several different cell types were efficiently transfected. Suicide therapies, such as through HSV-TK transfection, or reconstitution of apoptosis pathways would in this case be unsuitable [54].

Upon systemic delivery, cationic delivery vectors accumulate in the liver and spleen. To improve targeting in the context of ovarian cancer, folate is often used as a targeting agent since many ovarian tumors show high folate receptor expression. Several folate receptor targeting drugs are currently under investigation [55], but some failed after promising initial results [56]. Even with targeting moieties, many oligonucleotide delivery vectors still show major uptake in other organs [8]. Several authors therefore claim that the lack of cell specific uptake is a major obstacle in mRNA delivery for therapeutic protein expression that should be overcome before clinical implementation of mRNA therapies [57,58]. Most current clinical trials focus on mRNA vaccination, which is not subjected to this problem [26].

We propose a very different approach. Rather than tweaking target cell preference with targeting agents, we propose to opportunistically build on the intrinsic cellular preference of the nanoparticles combined with the appropriate route of delivery. Transient protein expression in the peritoneal cavity could greatly benefit immunotherapy. In ovarian cancer, local suppression of the immune system creates an environment in which the tumor escapes elimination and proliferates in the abdominal cavity [59,60]. High levels of $CD8^+$ cells are, however, positively correlated with patient survival in ovarian cancer [61–63]. Furthermore, adoptive allogeneic NK cell transfer shows promising results [42]. Candidate proteins would thus be stimulatory cytokines to boost a local immune response within the TME.

Clearly, at this point, the *in vivo* studies were explorative in nature. However, we have learned already at this point, that due to the heterogeneity of the starting material, quantitative analyses with respect to the targeted cell types will be challenging. The same applies to the tumor explants. Nevertheless, the diversity of cell types reached by either approach was fully consistent, supporting the validity of our conclusions.

In conclusion, PF14 is an efficient mRNA delivery vehicle that is able to target different cell types within the TME. It greatly outperforms a commercially available lipid formulation *in vivo*, and transfection was observed in different cell types of primary ovarian cancer explants. Thus, PF14 could be a suitable transfection agent for clinical applications regarding the delivery of mRNA in the context of ovarian cancer.

Declaration of Competing Interest

A. H. van Asbeck and R. Brock are cofounders of Mercurna, a company aimed at mRNA-based products.

Acknowledgement

M.A.J.G. was supported by a grant from the Netherlands Organisation for Scientific Research (NWO-Vici 916.14.655).

Appendix A. Supplementary material

Supplementary data to this article can be found online at https://doi.org/10.1016/j.ejpb.2019.05.014.

References

[1] L.A. Torre, F. Bray, R.L. Siegel, J. Ferlay, J. Lortet-Tieulent, A. Jemal, Global cancer statistics, 2012: Global Cancer Statistics, 2012, CA: Cancer J. Clin. 65 (2) (2015) 87–108, https://doi.org/10.3322/caac.21262.
[2] G.C. Jayson, E.C. Kohn, H.C. Kitchener, J.A. Ledermann, Ovarian cancer, The Lancet 384 (9951) (2014) 1376–1388, https://doi.org/10.1016/S0140-6736(13)62146-7.
[3] C. Orbegoso, G. Marquina, A. George, S. Banerjee, The role of Cediranib in ovarian cancer, Exp. Opin. Pharmacother. 18 (2017) 1637–1648.
[4] E. Pujade-Lauraine, F. Hilpert, B. Weber, A. Reuss, A. Poveda, G. Kristensen, R. Sorio, I. Vergote, P. Witteveen, A. Bamias, D. Pereira, P. Wimberger, A. Oaknin, M.R. Mirza, P. Follana, D. Bollag, I. Ray-Coquard, Bevacizumab combined with chemotherapy for platinum-resistant recurrent ovarian cancer: The AURELIA Open-Label Randomized Phase III Trial, J. Clin. Oncol. 32 (2014) 1302–1308.
[5] A.M. Oza, A.D. Cook, J. Pfisterer, A. Embleton, J.A. Ledermann, E. Pujade-Lauraine, G. Kristensen, M.S. Carey, P. Beale, A. Cervantes, T.-W. Park-Simon, G. Rustin, F. Joly, M.R. Mirza, M. Plante, M. Quinn, A. Poveda, G.C. Jayson, D. Stark, A.M. Swart, L. Farrelly, R. Kaplan, M.K.B. Parmar, T.J. Perren, Standard chemotherapy with or without bevacizumab for women with newly diagnosed ovarian cancer (ICON7): overall survival results of a phase 3 randomised trial, Lancet Oncol. 16 (2015) 928–936.
[6] A.J. Wiggans, G.K.S. Cass, A. Bryant, T.A. Lawrie, J. Morrison, Poly(ADP-ribose) polymerase (PARP) inhibitors for the treatment of ovarian cancer, Cochrane Database Syst. Rev., 2015.
[7] B. Ataseven, L.M. Chiva, P. Harter, A. Gonzalez-Martin, A. du Bois, FIGO stage IV epithelial ovarian, fallopian tube and peritoneal cancer revisited, Gynecol. Oncol. 142 (2016) 597–607.
[8] D. van den Brand, V. Mertens, L.F.A.G. Massuger, R. Brock, siRNA in ovarian cancer – delivery strategies and targets for therapy, J. Control. Release 283 (2018) 45–58.
[9] X. Yang, A.K. Iyer, A. Singh, L. Milane, E. Choy, F.J. Hornicek, M.M. Amiji, Z. Duan, Cluster of Differentiation 44 Targeted Hyaluronic Acid Based Nanoparticles for MDR1 siRNA Delivery to Overcome Drug Resistance in Ovarian Cancer, Pharm. Res. 32 (2015) 2097–2109.
[10] K.M. Gharpure, K.S. Chu, C.J. Bowerman, T. Miyake, S. Pradeep, S.L. Mangala, H.D. Han, R. Rupaimoole, G.N. Armaiz-Pena, T.B. Rahhal, S.Y. Wu, J.C. Luft, M.E. Napier, G. Lopez-Berestein, J.M. DeSimone, A.K. Sood, Metronomic docetaxel in PRINT nanoparticles and EZH2 silencing have synergistic antitumor effect in ovarian cancer, Mol. Cancer Ther. 13 (2014) 1750–1757.
[11] M.S. Goldberg, D. Xing, Y. Ren, S. Orsulic, S.N. Bhatia, P.A. Sharp, Nanoparticle-mediated delivery of siRNA targeting Parp1 extends survival of mice bearing tumors derived from Brca1-deficient ovarian cancer cells, Proc. Natl. Acad. Sci. USA 108 (2011) 745–750.
[12] M.M. Shahzad, L.S. Mangala, H.D. Han, C. Lu, J. Bottsford-Miller, M. Nishimura, E.M. Mora, J.W. Lee, R.L. Stone, C.V. Pecot, D. Thanapprapasr, J.W. Roh, P. Gaur, M.P. Nair, Y.Y. Park, N. Sabnis, M.T. Deavers, J.S. Lee, L.M. Ellis, G. Lopez-Berestein, W.J. McConathy, L. Prokai, A.G. Lacko, A.K. Sood, Targeted delivery of small interfering RNA using reconstituted high-density lipoprotein nanoparticles, Neoplasia 13 (2011) 309–319.
[13] G. Salzano, G. Navarro, M.S. Trivedi, G. De Rosa, V.P. Torchilin, Multifunctional polymeric micelles co-loaded with Anti-Survivin siRNA and Paclitaxel overcome drug resistance in an animal model of ovarian cancer, Mol. Cancer Ther. 14 (2015) 1075–1084.
[14] V. Shah, O. Taratula, O.B. Garbuzenko, O.R. Taratula, L. Rodriguez-Rodriguez, T. Minko, Targeted nanomedicine for suppression of CD44 and simultaneous cell death induction in ovarian cancer: an optimal delivery of siRNA and anticancer drug, Clin. Cancer Res. 19 (2013) 6193–6204.
[15] Y.H. Huang, W. Peng, N. Furuuchi, J. Gerhart, K. Rhodes, N. Mukherjee, M. Jimbo, G.E. Gonye, J.R. Brody, R.C. Getts, J.A. Sawicki, Delivery of therapeutics targeting the mRNA-Binding Protein HuR Using 3DNA nanocarriers suppresses ovarian tumor growth, Cancer Res. 76 (2016) 1549–1559.
[16] J.A. Wolff, R.W. Malone, P. Williams, W. Chong, G. Acsadi, A. Jani, P.L. Felgner, Direct gene transfer into mouse muscle in vivo, Science 247 (1990) 1465.
[17] R.D. Alvarez, J. Gomez-Navarro, M. Wang, M.N. Barnes, T.V. Strong, R.B. Arani, W. Arafat, J.V. Hughes, G.P. Siegal, D.T. Curiel, Adenoviral-mediated suicide gene

therapy for ovarian cancer, Mol. Ther. 2 (2000) 524–530.
[18] J.K. Wolf, A.D. Jenkins, Gene therapy for ovarian cancer (review), Int. J. Oncol. 21 (2002) 461–468.
[19] A.G. Zeimet, C. Marth, Why did p53 gene therapy fail in ovarian cancer? Lancet Oncol. 4 (2003) 415–422.
[20] M. Cavazzana, E. Six, C. Lagresle-Peyrou, I. André-Schmutz, S. Hacein-Bey-Abina, Gene therapy for X-linked severe combined immunodeficiency: where do we stand? Hum. Gene Ther. 27 (2016) 108–116.
[21] U. Sahin, K. Karikó, Ö. Türeci, mRNA-based therapeutics — developing a new class of drugs, Nat. Rev. Drug Discov. 13 (2014) 759.
[22] M. Alberer, U. Gnad-Vogt, H.S. Hong, K.T. Mehr, L. Backert, G. Finak, R. Gottardo, M.A. Bica, A. Garofano, S.D. Koch, M. Fotin-Mleczek, I. Hoerr, R. Clemens, F. von Sonnenburg, Safety and immunogenicity of a mRNA rabies vaccine in healthy adults: an open-label, non-randomised, prospective, first-in-human phase 1 clinical trial, The Lancet 390 (2017) 1511–1520.
[23] A. Thess, S. Grund, B.L. Mui, M.J. Hope, P. Baumhof, M. Fotin-Mleczek, T. Schlake, Sequence-engineered mRNA without chemical nucleoside modifications enables an effective protein therapy in large animals, Mol. Ther. 23 (2015) 1456–1464.
[24] L. Carlsson, J.C. Clarke, C. Yen, F. Gregoire, T. Albery, M. Billger, A.-C. Egnell, L.-M. Gan, K. Jennbacken, E. Johansson, G. Linhardt, S. Martinsson, M.W. Sadiq, N. Witman, Q.-D. Wang, C.-H. Chen, Y.-P. Wang, S. Lin, B. Ticho, P.C.H. Hsieh, K.R. Chien, R. Fritsche-Danielson, Biocompatible, Purified VEGF-A mRNA Improves Cardiac Function after Intracardiac Injection 1 Week Post-myocardial Infarction in Swine, Mol. Ther. Methods Clin. Dev. 9 (2018) 330–346.
[25] K. Bahl, J.J. Senn, O. Yuzhakov, A. Bulychev, L.A. Brito, K.J. Hassett, M.E. Laska, M. Smith, Ö. Almarsson, J. Thompson, A. Ribeiro, M. Watson, T. Zaks, G. Ciaramella, Preclinical and Clinical Demonstration of Immunogenicity by mRNA Vaccines against H10N8 and H7N9 Influenza Viruses, Mol. Ther. 25 (2017) 1316–1327.
[26] K.A. Hajj, K.A. Whitehead, Tools for translation: non-viral materials for therapeutic mRNA delivery, Nat. Rev. Mater. 2 (2017) 17056.
[27] D. van den Brand, C. Veelken, L. Massuger, R. Brock, Penetration in 3D tumor spheroids and explants: Adding a further dimension to the structure-activity relationship of cell-penetrating peptides, Biochim. Biophys. Acta (BBA) – Biomembr. 1860 (2018) 1342–1349.
[28] A.K. Varkouhi, M. Scholte, G. Storm, H.J. Haisma, Endosomal escape pathways for delivery of biologicals, J. Control. Release 151 (2011) 220–228.
[29] Z. Meng, J. O'Keeffe-Ahern, J. Lyu, L. Pierucci, D. Zhou, W. Wang, A new developing class of gene delivery: messenger RNA-based therapeutics, Biomater. Sci. 5 (2017) 2381–2392.
[30] O. Boussif, F. Lezoualc'h, M.A. Zanta, M.D. Mergny, D. Scherman, B. Demeneix, J.P. Behr, A versatile vector for gene and oligonucleotide transfer into cells in culture and in vivo: polyethylenimine, Proc. Natl. Acad. Sci. USA 92 (1995) 7297–7301.
[31] F. Milletti, Cell-penetrating peptides: classes, origin, and current landscape, Drug Discov. Today 17 (2012) 850–860.
[32] P. Lundin, H. Johansson, P. Guterstam, T. Holm, M. Hansen, Ü. Langel, S. El Andaloussi, Distinct uptake routes of cell-penetrating peptide conjugates, Bioconjug. Chem. 19 (2008) 2535–2542.
[33] A.H. van Asbeck, A. Beyerle, H. McNeill, P.H.M. Bovee-Geurts, S. Lindberg, W.P.R. Verdurmen, M. Hällbrink, Ü. Langel, O. Heidenreich, R. Brock, Molecular parameters of siRNA–Cell penetrating peptide nanocomplexes for efficient cellular delivery, ACS Nano 7 (2013) 3797–3807.
[34] K. Ezzat, S. El Andaloussi, E.M. Zaghloul, T. Lehto, S. Lindberg, P.M.D. Moreno, J.R. Viola, T. Magdy, R. Abdo, P. Guterstam, R. Sillard, S.M. Hammond, M.J.A. Wood, A.A. Arzumanov, M.J. Gait, C.I.E. Smith, M. Hällbrink, Ü. Langel, PepFect 14, a novel cell-penetrating peptide for oligonucleotide delivery in solution and as solid formulation, Nucl. Acids Res. 39 (2011) 5284–5298.
[35] K. Ezzat, E.M. Zaghloul, S. El Andaloussi, T. Lehto, R. El-Sayed, T. Magdy, C.I.E. Smith, Ü. Langel, Solid formulation of cell-penetrating peptide nanocomplexes with siRNA and their stability in simulated gastric conditions, J. Control. Release 162 (2012) 1–8.
[36] K.-L. Veiman, I. Mäger, K. Ezzat, H. Margus, T. Lehto, K. Langel, K. Kurrikoff, P. Arukuusk, J. Suhorutšenko, K. Padari, M. Pooga, T. Lehto, Ü. Langel, PepFect14 peptide vector for efficient gene delivery in cell cultures, Mol. Pharm. 10 (2013) 199–210.
[37] H. Shen, C. Rodriguez-Aguayo, R. Xu, V. Gonzalez-Villasana, J. Mai, Y. Huang, G. Zhang, X. Guo, L. Bai, G. Qin, X. Deng, Q. Li, D.R. Erm, B. Aslan, X. Liu, J. Sakamoto, A. Chavez-Reyes, H.D. Han, A.K. Sood, M. Ferrari, G. Lopez-Berestein, Enhancing chemotherapy response with sustained EphA2 silencing using multistage vector delivery, Clin. Cancer Res. 19 (2013) 1806–1815.
[38] W. Chen, Y. Yuan, D. Cheng, J. Chen, L. Wang, X. Shuai, Co-Delivery of Doxorubicin and siRNA with reduction and pH dually sensitive nanocarrier for synergistic cancer therapy, Small 10 (2014) 2678–2687.
[39] M. Talekar, Q. Ouyang, M.S. Goldberg, M.M. Amiji, Cosilencing of PKM-2 and MDR-1 sensitizes multidrug-resistant ovarian cancer cells to paclitaxel in a murine model of ovarian cancer, Mol. Cancer Ther. 14 (2015) 1521–1531.
[40] C. He, D. Liu, W. Lin, Self-assembled nanoscale coordination polymers carrying siRNAs and cisplatin for effective treatment of resistant ovarian cancer, Biomaterials 36 (2015) 124–133.
[41] E. Collado Camps, R. Brock, An opportunistic route to success: Towards a change of paradigm to fully exploit the potential of cell-penetrating peptides, Bioorg. Med. Chem. (2017).
[42] J.S. Hoogstad- van Evert, J. Cany, D. van den Brand, M. Oudenampsen, R. Brock, R. Torensma, R.L. Bekkers, J.H. Jansen, L.F. Massuger, H. Dolstra, Umbilical cord blood CD34+ progenitor-derived NK cells efficiently kill ovarian cancer spheroids and intraperitoneal tumors in NOD/SCID/IL2Rgnull mice, OncoImmunology (2017) 00 00.
[43] M.J. Vallen, S. Schmidt, A. Oosterhof, J. Bulten, L.F. Massuger, T.H. van Kuppevelt, Primary ovarian carcinomas and abdominal metastasis contain 4,6-disulfated chondroitin sulfate rich regions, which provide adhesive properties to tumour cells, PLoS ONE 9 (2014) e111806.
[44] M.-T. Ke, S. Fujimoto, T. Imai, SeeDB: a simple and morphology-preserving optical clearing agent for neuronal circuit reconstruction, Nat. Neurosci. 16 (2013) 1154.
[45] K.-L. Veiman, K. Künnapuu, T. Lehto, K. Kiisholts, K. Pärn, Ü. Langel, K. Kurrikoff, PEG shielded MMP sensitive CPPs for efficient and tumor specific gene delivery in vivo, J. Control. Release 209 (2015) 238–247.
[46] K.A.T. Naipal, N.S. Verkaik, H. Sánchez, C.H.M. van Deurzen, M.A. den Bakker, J.H.J. Hoeijmakers, R. Kanaar, M.P.G. Vreeswijk, A. Jager, D.C. van Gent, Tumor slice culture system to assess drug response of primary breast cancer, BMC Cancer 16 (2016) 78.
[47] V.K. Udhayakumar, A. De Beuckelaer, J. McCaffrey, C.M. McCrudden, J.L. Kirschman, D. Vanover, L. Van Hoecke, K. Roose, K. Deswarte, B.G. De Geest, S. Lienenklaus, P.J. Santangelo, J. Grooten, H.O. McCarthy, S. De Koker, Arginine-rich peptide-based mRNA Nanocomplexes Efficiently Instigate Cytotoxic T Cell Immunity Dependent on the amphipathic organization of the peptide, Adv. Healthc. Mater. 6 (2017).
[48] S.T. Crowley, J.A. Poliskey, N.J. Baumhover, K.G. Rice, Efficient expression of stabilized mRNA PEG-peptide polyplexes in liver, Gene Ther. 22 (2015) 993–999.
[49] K. Kurrikoff, K.-L. Veiman, K. Künnapuu, E.M. Peets, T. Lehto, L. Pärnaste, P. Arukuusk, Ü. Langel, Effective in vivo gene delivery with reduced toxicity, achieved by charge and fatty acid -modified cell penetrating peptide, Sci. Rep. 7 (2017) 17056.
[50] C.J. McKinlay, J.R. Vargas, T.R. Blake, J.W. Hardy, M. Kanada, C.H. Contag, P.A. Wender, R.M. Waymouth, Charge-altering releasable transporters (CARTs) for the delivery and release of mRNA in living animals, Proc. Natl. Acad. Sci. 114 (2017) E448.
[51] T.T. Goodman, P.L. Olive, S.H. Pun, Increased nanoparticle penetration in collagenase-treated multicellular spheroids, Int. J. Nanomed. 2 (2007) 265.
[52] K. Huang, H. Ma, J. Liu, S. Huo, A. Kumar, T. Wei, X. Zhang, S. Jin, Y. Gan, P.C. Wang, S. He, X. Zhang, X.-J. Liang, Size-dependent localization and penetration of ultrasmall gold nanoparticles in cancer cells,multicellular spheroids, and tumors in Vivo, ACS Nano 6 (2012) 4483–4493.
[53] K.N. Sugahara, T. Teesalu, P.P. Karmali, V.R. Kotamraju, L. Agemy, D.R. Greenwald, E. Ruoslahti, Coadministration of a tumor-penetrating peptide enhances the efficacy of cancer drugs, Science 328 (2010) 1031.
[54] Z. Karjoo, X. Chen, A. Hatefi, Progress and problems with the use of suicide genes for targeted cancer therapy, Adv. Drug Deliv. Rev. 99 (2016) 113–128.
[55] A. Bergamini, S. Ferrero, U. Leone Roberti Maggiore, C. Scala, F. Pella, V.G. Vellone, M. Petrone, E. Rabaiotti, R. Cioffi, M. Candiani, G. Mangili, Folate receptor alpha antagonists in preclinical and early stage clinical development for the treatment of epithelial ovarian cancer, Exp. Opin. Invest. Drugs 25 (2016) 1405–1412.
[56] I.B. Vergote, L.G. Gilbert, P. Lucy, A. Ghatage, S. Lisyankaya, S.K. Ghamande, J.A. Chambers, D.M. Arranz, P. Provencher, A. Bessette, J. Amnon, R.T. Symanowski, R.W. Penson, R. Clark Naumann, A randomized double-blind phase III trial comparing vintafolide (EC145) and pegylated liposomal doxorubicin (PLD/Doxil®/Caelyx®) in combination versus PLD in participants with platinum-resistant ovarian cancer (PROCEED) (NCT01170650), Gynecol. Oncol. 137 (2015) 5–6.
[57] M.G. Stanton, Current status of messenger RNA delivery systems, Nucl. Acid Ther. (2018).
[58] B. Li, X. Zhang, Y. Dong, Nanoscale platforms for messenger RNA delivery, Wiley Interdiscip. Rev. Nanomed. Nanobiotechnol. (2018) e1530.
[59] C. Wefers, T. Duiveman-de Boer, L.P. Zusterzeel, F.L. Massuger, D. Fuchs, R. Torensma, E.C. Wheelock, J.I. de Vries, Different lipid regulation in ovarian cancer: inhibition of the immune system, Int. J. Mol. Sci. 19 (2018).
[60] R. Yigit, L.F.A.G. Massuger, C.G. Figdor, R. Torensma, Ovarian cancer creates a suppressive microenvironment to escape immune elimination, Gynecol. Oncol. 117 (2010) 366–372.
[61] B. Clarke, A.V. Tinker, C.-H. Lee, S. Subramanian, M. van de Rijn, D. Turbin, S. Kalloger, G. Han, K. Ceballos, M.G. Cadungog, D.G. Huntsman, G. Coukos, C.B. Gilks, Intraepithelial T cells and prognosis in ovarian carcinoma: novel associations with stage, tumor type, and BRCA1 loss, Mod. Pathol. 22 (2008) 393.
[62] E. Sato, S.H. Olson, J. Ahn, B. Bundy, H. Nishikawa, F. Qian, A.A. Jungbluth, D. Frosina, S. Gnjatic, C. Ambrosone, J. Kepner, T. Odunsi, G. Ritter, S. Lele, Y.-T. Chen, H. Ohtani, L.J. Old, K. Odunsi, Intraepithelial $CD8^+$ tumor-infiltrating lymphocytes and a high $CD8^+$/regulatory T cell ratio are associated with favorable prognosis in ovarian cancer, PNAS 102 (2005) 18538.
[63] J.R. Webb, D.A. Wick, J.S. Nielsen, E. Tran, K. Milne, E. McMurtrie, B.H. Nelson, Profound elevation of CD8+ T cells expressing the intraepithelial lymphocyte marker CD103 (αE/β7 Integrin) in high-grade serous ovarian cancer, Gynecol. Oncol. 118 (2010) 228–236.